Available online at www.sciencedirect.com
ScienceDirect
Applied Surface Science 253 (2007) 4390–4395
applied surface science
www.elsevier.com/locate/apsusc

Study on the mechanisms of photoinduced carriers separation and recombination for Fe^{3+}–TiO_2 photocatalysts

Baifu Xin [a,b], Zhiyu Ren [a], Peng Wang [b], Jia Liu [a], Liqiang Jing [a], Honggang Fu [a,*]

[a] School of Chemistry and Materials Science, Heilongjiang University, Xue Fu Road No.74, Nan-gang, Harbin 150080, PR China
[b] School of Municipal and Environmental Engineering, Harbin Institute of Technology, Harbin 150090, PR China

Received 6 October 2005; received in revised form 14 May 2006; accepted 25 September 2006
Available online 25 October 2006

Abstract

The iron(III)-ion doped TiO_2 (Fe^{3+}–TiO_2) with different doping Fe^{3+} content were prepared via a sol–gel method. The as-prepared Fe^{3+}–TiO_2 nanoparticles were investigated by means of surface photovoltage spectroscopy (SPS), field-induced surface photovoltage spectroscopy (FISPS), and the photoelectrochemical properties of Fe^{3+}–TiO_2 catalysts with different Fe^{3+} content are performed by electrical impedance spectroscopy (EIS) as well as photocatalytic degradation of RhB are studied under illuminating. Based on the experiment results, the mechanism of photoinduced carriers separation and recombination of Fe^{3+}–TiO_2 was revealed: that is, the Fe^{3+} captures the photoinduced electrons, inhibiting the recombination of photoinduced electron–hole pairs, this favors to the photocatalytic reaction at low doping concentration (Fe/Ti $\leq$ 0.03 mol%); while Fe^{3+} dopant content exceeds 0.03 mol%, Fe_2O_3 became the recombination centers of photoinduced electrons and holes because of that the interaction of Fe_2O_3 with TiO_2 leads to that the photoinduced electrons and holes of TiO_2 transfer to Fe_2O_3 and recombine quickly, which is unfavorable to the photocatalytic reaction.

PACS : 73.50.Pz; 73.90.+f; 84.37.+q

Keywords: Fe^{3+} doped TiO_2; Photocatalysis; Photoinduced carrier characteristics

1. Introduction

Titanium dioxide is broadly used as a photocatalyst because it is photochemically stable, non-toxic and cost little [1–5]. However, the efficiency of photocatalytic reactions is limited by the high recombination rate of photoinduced electron–hole pairs formed in photocatalytic processes and by the absorption capability for visible light of photocatalysts. Many studies have been devoted to the improvement of photocatalytic efficiency of TiO_2, such as depositing noble metals [6–14] and doping metal or non-metal ions [15–22]. In particular, Fe^{3+}–TiO_2 has been the topic of many investigation including preparation, characterization, dynamics of charge transfer, trapping and recombination, and photocatalytic behavior, etc. [23–35]. In these studies, however, the recombination mechanism of photoinduced carriers of Fe^{3+}–TiO_2 has not been distinct. All reports referring to the recombination mechanisms are devoid of sufficient experimental evidence.

The surface photovoltage (SPV) method is a well-established contactless technique for the characterization of semiconductors, which relies on analyzing photoinduced changes in the surface voltage [36,37]. Signal of SPS is variational value of surface voltage before and after illumination during the test. It is a powerful tool for semiconductor surface characterization. It can offer important information about semiconductor surface, interface and bulk properties, including: surface band bending; surface and bulk carrier recombination; surface state distribution, etc., mainly reflecting the carrier separation and transfer behavior with the aid of light [36], especially when the SPS technique is combined with the electric field-modified technique [38]. The sensitivity of this method is about $10^8 q/cm^2$, or about one elementary charge per 10^7 surface atoms [39]. It is obvious that SPS is more sensitive than X-ray photoelectron or Auger spectroscopy, which makes its scope of applications wider [40].

* Corresponding author. Tel.: +86 451 86608458; fax: +86 451 86673647.
E-mail address: fuhg@vip.sina.com (H. Fu).

0169-4332/$ – see front matter © 2006 Elsevier B.V. All rights reserved.
doi:10.1016/j.apsusc.2006.09.049

Electrochemical impedance spectroscopy (EIS) is a very important technology for studying the mechanism and kinetics of complicated electrode reaction. EIS data is generally analyzed in terms of an equivalent circuit model. By fitting of this impedance spectrum to a model or an equivalent electrical circuit, we can obtain some information about electrochemical properties of TiO_2 catalysts.

In this work, TiO_2 photocatalysts with different doping Fe^{3+} content were prepared by the sol–gel method. The mechanisms of photoinduced carriers separation and recombination of Fe^{3+}–TiO_2 were investigated by means of SPS, FISPS and EIS.

2. Experimental

2.1. The preparation of Fe^{3+}–TiO_2 nanoparticles and electrodes

Specimens of Fe^{3+}–TiO_2 containing different amounts of Fe^{3+} were prepared by sol–gel method. 7.6 mL of $Ti(OBu_t)_4$ was dissolved in 5.5 mL of CH_3OH containing different amount of $Fe(NO_3)_3{\cdot}9H_2O$ under vigorous stirring. In order to control the hydrolyzation, 3 mL of CH_3COOH was added to the solution before suitable amount of water (2 mL) was added to it. The resulting transparent colloidal liquid was continuously stirred till the gel was formed. The gel was dried at 100 °C for 6 h, calcined at 400 °C for 2 h in air and ground to obtain the Fe^{3+}–TiO_2 nanoparticles. The Fe^{3+} concentrations in the samples were 0, 0.01, 0.03, 0.05, 0.1, 0.3, 0.5, 1, 3, 5 mol%, respectively.

The organic pastes of Fe^{3+}–TiO_2 are prepared as follow steps: 0.01 mL of acetylacetone, 0.05 mL of 10 wt% OP-10 and 1 mL of 20 wt% PEG-20 M are added to 4 mL of deionized water, then the above mixture solution are added to 1 g as-prepared Fe^{3+}–TiO_2 nanoparticles in an agate mortar while grinding with an agate pestle. The electrodes of Fe^{3+}–TiO_2 are prepared by spreading above paste of Fe^{3+}–TiO_2 on the ITO glass (<15 Ω/square) by means of a doctor-blade method reported by Smestad and Gratzel [41]. After sintering at 450 °C in air for 30 min, the electrodes of Fe^{3+}–TiO_2 with different Fe^{3+} content can be obtained.

2.2. Characterization of samples

TiO_2 and Fe^{3+}–TiO_2 powders were examined by Raman spectra of Renishaw RM1000 excited at 514.5 nm. XPS spectra was recorded with an Escalab MK II (VG Company, UK). All binding energies (BE) were calibrated by the BE (284.6 eV) of C1s, which gave BE values within an accuracy of ±0.1 eV. Energy dispersive X-ray spectroscopy (EDS) was recorded on a KYKY2000 SEM. The SPS instrument was assembled at Jilin University, monochromatic light was obtained by passing light from a 500 W xenon lamp (CHF-XQ500W, China) through a double-prism monochromator (SBP300, China). The slit widths of entrance and exit were 2 and 1 mm, respectively. A lock-in amplifier (SR830, USA), synchronized with a light chopper (SR540, USA), was employed to amplify the photovoltage signal. The powder sample is sandwiched between two ITO glass electrodes.

The EIS test are performed in a three-electrode system, in which Fe^{3+}–TiO_2/ITO electrodes with different Fe^{3+} content act as the working electrode (area 1.2 cm^2), Saturated calomel electrode (SCE) and platinum sheet (area 2 cm^2) are used as the reference electrode and the auxiliary electrode, respectively. A 160 W high-pressure mercury lamp is used as the light source, illumination being from the TiO_2 side. An IM6e impedance analyzer (ZAHNER-electrik) is used to perform the EIS test. The frequencies for EIS measurement are scanned from 10^5 to 0.1 Hz using a perturbation of 50 mV over the open circuit potential and without any applied dc voltage. The experimental data are analyzed using the IM6e system software. The solution used for EIS test is 10 mg/L RhB with 500 mg/L KCl. The pH of test solution is 6.

2.3. Evaluation of photocatalytic activity of Fe^{3+}–TiO_2

The photocatalytic degradation of RhB over Fe^{3+}–TiO_2 was carried out in an home-built reactor. A 160 W high-pressure mercury lamp was used as light source, whose intensity was 17.1 mW/cm^2. In each run 0.15 g Fe^{3+}–TiO_2 catalyst was added into 20 mL RhB solution of 10 mg/L. After premixing for 20 min, the light was turned on to initiate the reaction. A HITACHI U-2000 UV–vis spectrometer was used to determine the concentration of RhB solution before and after photocatalytic degradation.

3. Results and discussion

3.1. Characterization of Fe^{3+}–TiO_2

The Raman spectrum for TiO_2 and the 5 mol% Fe^{3+}–TiO_2 (Fig. 1) show peaks at 144, 397, 516 and 639 cm^{-1}. The bands at 639 cm^{-1} and about 144 cm^{-1} are assigned to the E_g modes and the band at 397 cm^{-1} to the B_{1g} mode of TiO_2 anatase. The band at 516 cm^{-1} is a doublet of A_{1g} and B_{1g} [42]. There are no peaks that indicate the presence of Fe_2O_3 within the limit of detection after iron ion doping. However, the EDS spectra of the 5 mol% Fe–TiO_2 sample (Fig. 2) shows that there is iron

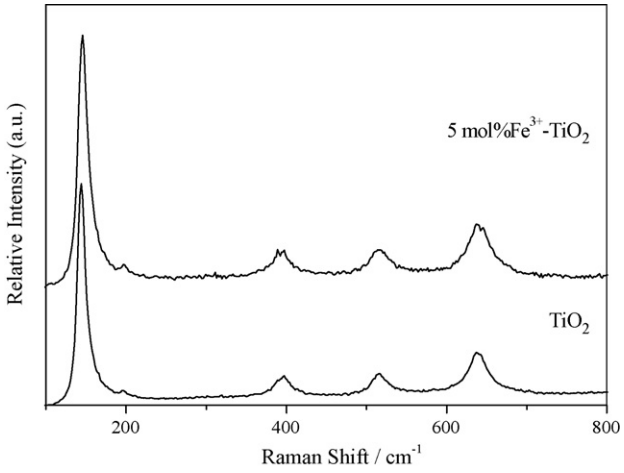

Fig. 1. Raman spectra of TiO_2 and the 5 mol% Fe^{3+}–TiO_2 samples.

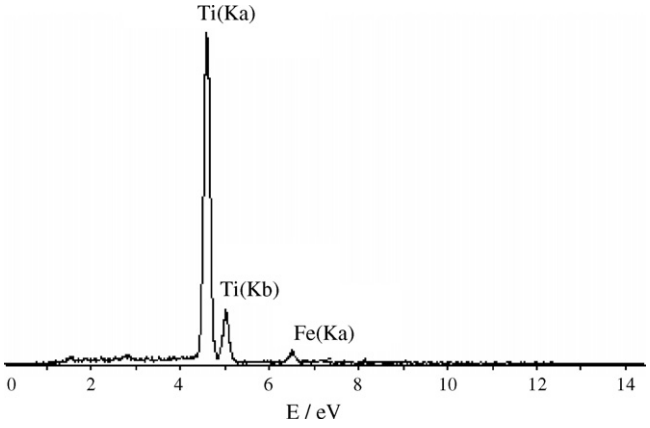

Fig. 2. EDS spectra of the 5 mol% Fe^{3+}–TiO_2.

Table 1
Raman shift and FWHM of TiO_2 and the 5 mol% Fe^{3+}–TiO_2 samples

TiO_2				
Raman shift (cm^{-1})	144.2	397.4	515.5	639.1
FWHM (cm^{-1})	12.1	24.6	22.4	27.8
5 mol% Fe^{3+}–TiO_2				
Raman shift (cm^{-1})	145.1	398.9	516.8	640.8
FWHM (cm^{-1})	14.5	26.2	28.9	31.8

element in the sample. This means that Fe_2O_3 dispersed uniformly in the bulk of TiO_2, and did not form the continuous phase of Fe_2O_3. From Fig. 1 and Table 1, a broadening of the Raman bands can be observed for the doped one. The reasons for this fact maybe have two factors: one is due to a small crystal size; another is due to the distortion of crystal lattice. Our previous work suggested that the crystal size of doped samples (10.25 nm) are not obviously decreased comparing with the pure TiO_2 (11.48 nm) [43]. So this broadening mainly originates from that doped iron ions diffuse into the crystal lattice of TiO_2 because atom radius of Fe^{3+} and Ti^{4+} are very closed, which results in the variation of the structure of the crystal lattice and decrease of crystal symmetry, leading to cleavage of vibration phonon modes.Fig. 3 shows XPS spectra of Ti 2p of TiO_2 and the 5 mol% Fe–TiO_2. Form Fig. 3 we can see, the Ti 2p binding energy of the 5 mol% Fe–TiO_2 sample is increased in compared with that of pure TiO_2. This is because that the Fermi level of Fe_2O_3 is lower than that of TiO_2 so that the electrons of TiO_2 can transfer to highly dispersed Fe_2O_3 in TiO_2, which results in decrease in the outer electron cloud density of Ti ions. This fact suggests that there is an intense interaction between TiO_2 and Fe_2O_3.

3.2. Mechanisms of photoinduced carriers separation and recombination

Figs. 4 and 5 show the SPS and FISPS spectra of the pure TiO_2 and Fe^{3+}–TiO_2 contain different Fe^{3+} content without and with 0.6 V external electric field, respectively. In general, the SPS intensity relating to Fe_2O_3 is lower because that the recombination ratio of the photoinduced electron–hole pairs of Fe_2O_3 is very high [44], which results in that the SPS response of Fe_2O_3 cannot be seen, namely, we can only see one response originates from the band–band electron transition of TiO_2 at about 350 nm in Fig. 4. However, under an appropriate external electric field, the band–band electron transition of Fe_2O_3 can be promoted. So, the remarkable changes of SPS response from 400 to 550 nm assigned to the band–band electron transition of Fe_2O_3 [45] can occur in the presence of an external electric field as shown in Fig. 5. From Fig. 5, it can be seen: at lower Fe^{3+} content region ($\leq$0.03 mol%), we could only see one response originates from the band–band electron transition of TiO_2 at about 350 nm, which is decreased with increasing of the Fe^{3+} dopant content. This is because that Fe^{3+} dispersed uniformly in the bulk of TiO_2, which can capture the photoinduced electrons and holes transfer from bulk to surface, and generates Fe^{2+} and Fe^{4+}, respectively. This phenomena indicates that doping of Fe^{3+} at lower concentration region inhibits the recombination of photoinduced electron–hole pairs, and results in the photoresponse of TiO_2 decrease. When the Fe^{3+} dopant content exceeds 0.03 mol%, however, we can observe a new SPS signal from 400 to 550 nm assigned to the band–band electron transition of Fe_2O_3, which did not appear in absence of external electric field as shown in Fig. 4. Moreover, Fig. 5 shows that the characteristic response of TiO_2 at 350 nm gradually goes down, but that of Fe_2O_3 around

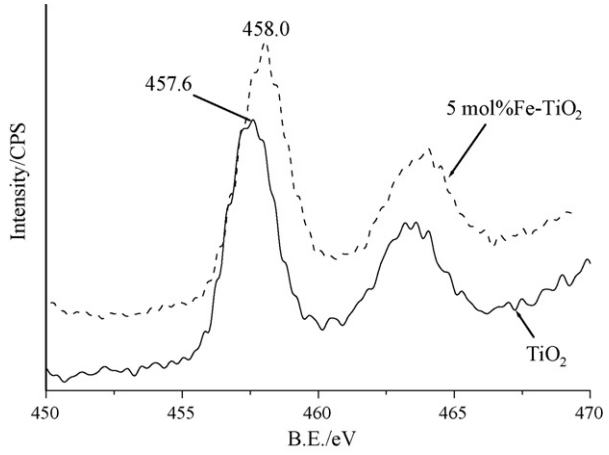

Fig. 3. XPS spectra of Ti 2p of TiO_2 and the 5 mol% Fe–TiO_2.

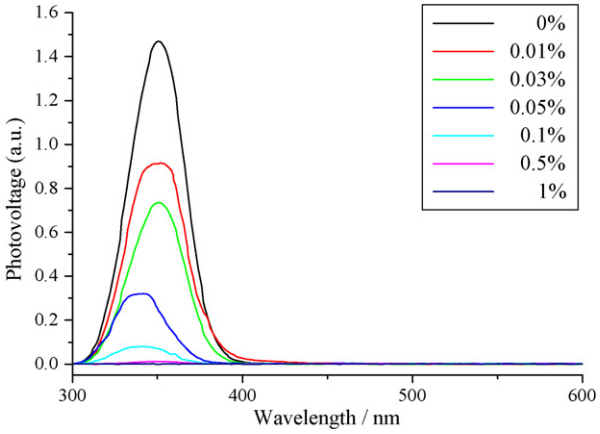

Fig. 4. SPS spectra of pure TiO_2 and Fe^{3+}–TiO_2 with different doping content.

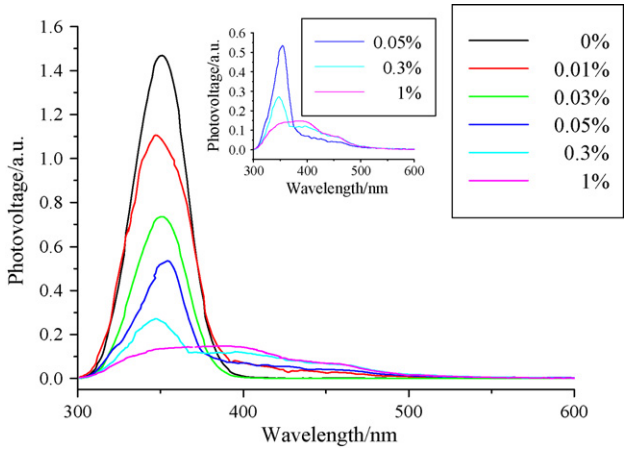

Fig. 5. FISPS spectra of pure TiO_2 and Fe^{3+}–TiO_2 with different doping content under 0.6 V external electric field.

400 nm increases with increase in Fe^{3+} dopant content. The main reasons for this phenomena are as follows: the amount of Fe_2O_3 increase with increase in Fe^{3+} dopant content (>0.03 mol%), so the photoresponse of Fe_2O_3 from 400 to 550 nm increased. Meanwhile, because of the level of conduction band of TiO_2 is higher than that of Fe_2O_3, but the level of valence band of TiO_2 is lower than that of Fe_2O_3, thus, when the phase of Fe_2O_3 forms, the electrons of conduction band and the holes of the valence band of TiO_2 can transfer to Fe_2O_3, then, these electrons and holes can recombine quickly, leading to the SPS signal at 350 nm depress continuously with increase in the Fe^{3+} dopant content. The experimental results suggests that Fe_2O_3 is recombination centers of photoinduced electrons and holes when Fe^{3+} dopant content exceeds 0.03 mol%.

The Nyquist plots of Fe^{3+}–TiO_2 with different Fe^{3+} content in 10 mg/L RhB solution with 500 mg/L KCl are shown in Fig. 6. It can be seen that, for the RhB photoelectrochemical degradation, only one arc can be observed on the EIS Nyquist plot, suggesting that such a degradation reaction appears to be a simple electrode reaction and electron transfer, hole transfer or

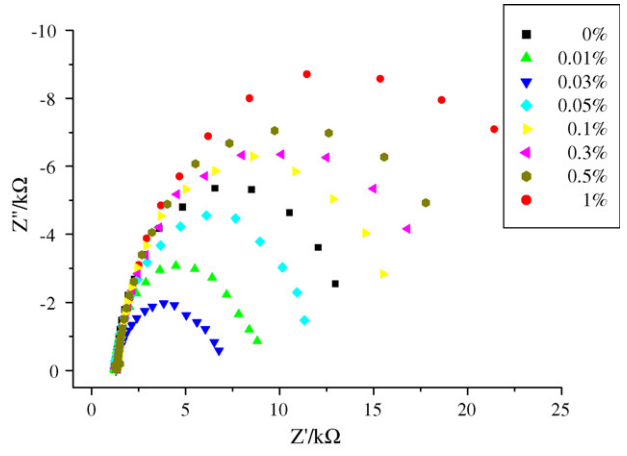

Fig. 6. EIS Nyquist plots of RhB photoelectrochemical degradations for Fe^{3+}–TiO_2 anodic film with different doping molar ratio: RhB concentration = 10 mg/L, KCl concentration = 500 mg/L, illumination, no bias, pH 6.

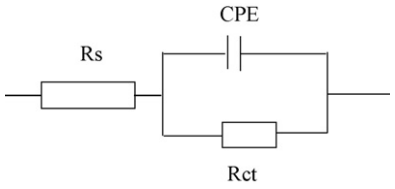

Fig. 7. The equivalent circuits of the 0.03 mol% Fe^{3+}–TiO_2 anodic film: R_s, the solution resistance; R_{ct}, the electron-transfer resistance; CPE, the constant phase element.

the recombination of electrons and holes is ''rate-determining'' [46]. The Equivalent circuit is obtained as shown in Fig. 7 and R_s is the solution resistance; R_{ct} is the electron-transfer resistance; CPE is the constant phase element, it is considered a capacitance of double layer here because the values of n are all close to 1. The fitting results for equivalent circuits of Fe^{3+}–TiO_2 with different Fe^{3+} content are shown in Table 2. From the Nyquist plots and the fitting results, it is found that the diameters of the semicircle and the values of R_{ct} decrease with increasing Fe^{3+} content, and the diameters of the semicircle and the values of R_{ct} of 0.03 mol% Fe^{3+} doped sample is the lower than that of others. However, when the Fe^{3+} dopant content exceed 0.03 mol%, the diameters of the semicircle and the values of R_{ct} increase. The size of the semicircle and the value of R_{ct} can demonstrate an effective separation of photogenerated electron–hole pairs [47] and the effective photoelectrocatalytic degradation of RhB.

The experimental results of EIS test obtain the same conclusion of SPS, namely, at lower Fe^{3+} dopant content region, Fe^{3+} acts as the traps of capture the photoinduced electrons and holes, and inhibit recombination of photoinduced electrons and holes, leading to photogenerated charge carrier concentration rise, so the diameters of the semicircle and the values of R_{ct} decrease. Otherwise, when the Fe^{3+} dopant content exceed 0.03 mol%, Fe_2O_3 become the recombination centers of photoinduced electrons and holes so that photogenerated charge carrier concentration decrease and the diameters of the semicircle and the values of R_{ct} increase.

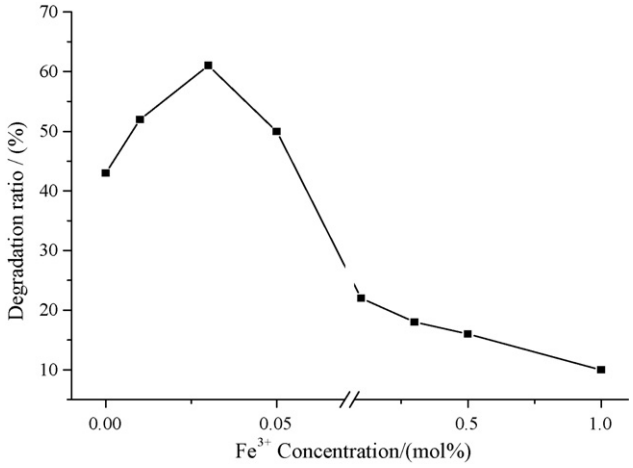

Fig. 8. Photocatalytic degradation ratio curve of RhB over different Fe^{3+}–TiO_2 photocatalysts.

Table 2
Fitting results for equivalent circuits of different doping molar ratio Fe^{3+}–TiO_2 anodic film

Parameters	Fe/Ti molar ratio							
	0%	0.01%	0.03%	0.05%	0.1%	0.3%	0.5%	1%
R_s (Ω)	9.82	14.45	14.96	10.27	12.64	11.37	10.03	8.46
R_{ct} (Ω)	2316	894.5	871.6	903.9	1092	3168	5640	18190
CPE (μf)	11.9	18.03	18.75	16.75	14.98	7.704	7.006	3.331
n	0.9121	0.8716	0.9156	0.9365	0.9583	0.8608	0.8343	0.9041

3.3. Evaluation of photocatalytic activity

Fig. 8 shows the photocatalytic degradation curves of RhB over Fe^{3+}–TiO_2 photocatalysts with different Fe^{3+} dopant content. It can be found that the photodegradation ratio of RhB is increased with increase in Fe^{3+} dopant content. Over 0.03 mol% Fe^{3+}–TiO_2, the degradation ratio of RhB is the highest. When the Fe^{3+} dopant content exceeds 0.03 mol%, however, the degradation ratio markedly go down. Which could be attributed to the following: appropriate amount of the doped Fe^{3+} ($\leq$0.03 mol%) in TiO_2 can effectively capture the photoinduced electrons and holes, which inhibits the combination of photoinduced carriers and improves the photocatalytic activity of photocatalysts. While Fe^{3+} dopant content exceeds 0.03 mol%, Fe_2O_3 becomes the recombination centers of the photoinduced electrons and holes, which is unfavorable to photocatalytic reactions. It can be seen that the photocatalytic activity well corresponds to the results of SPS and EIS discussed above. The mechanisms of photoinduced carriers separation and recombination mentioned above are further confirmed by the photocatalytic experimental evidence. This also demonstrate that there is a close relationship between the photocatalytic activity and the SPS and EIS measurements. So the activity of photocatalyst may be estimated by the SPS and EIS measurements.

4. Conclusion

The different doping ratio Fe^{3+}–TiO_2 were prepared by a sol–gel method. The mechanisms of photoinduced electrons and holes separation and recombination are investigated by SPS, FISPS and EIS measurements and photocatalytic reactions. The results reveal that Fe^{3+} acts as the traps to capture the photoinduced electrons, which inhibits the combination of photoinduced carriers and improves the photocatalytic activity of photocatalysts at low doping content ($\leq$0.03 mol%); while Fe^{3+} dopant content exceeds 0.03 mol%, Fe_2O_3 becomes the recombination centers of the photoinduced electrons and holes, which is unfavorable to photocatalytic reactions.

Acknowledgements

This project is supported from the Key Program Projects of National Natural Science Foundation of China (no. 20431030), the Program for New Century Excellent Talents in University (NCET-04-0341), the National Natural Science Foundation of China (no. 20301006), the Foundation for Excellent Youth of Heilongjiang Province (2002) and Heilongjiang University (2005), the Natural Science Foundation of Heilongjiang Province (no. B0305), for which the authors are very grateful.

References

[1] A. Fujishima, T.N. Rao, D.A. Tryk, J. Photochem. Photobiol. C 1 (2000) 1–21.
[2] Z.G. Zou, J.H. Ye, K. Sayama, H. Arakawa, Nature 414 (2001) 625–627.
[3] R. Asahi, T. Morikawa, T. Ohwaki, K. Aoki, Y. Taga, Science 293 (2001) 269–271.
[4] S. Malato, J. Caceres, A. Agüera, M. Mezcua, D. Hernando, J. Vial, A.R. Fernández-Alba, Environ. Sci. Technol. 35 (2001) 4359–4366.
[5] K. Nagaveni, G. Sivalingam, M.S. Hegde, G. Madras, Environ. Sci. Technol. 38 (2004) 1600–1604.
[6] M. Bowker, D. James, P. Stone, R. Bennett, N. Perkins, L. Millard, J. Greaves, A. Dickinson, J. Catal. 217 (2003) 427–433.
[7] Y.X. Li, G. Lu, S. Li, J. Photochem. Photobiol. A 152 (2002) 219–228.
[8] J.M. Herrmann, J. Disdier, P. Pichat, J. Catal. 113 (1988) 72–81.
[9] Y. Kohno, H. Hayashi, S. Takenaka, T. Tanaka, T. Funabiki, S. Yoshida, J. Photochem. Photobiol. A 126 (1999) 117–123.
[10] E. Stathatos, P. Lianos, P. Falaras, A. Siokou, Langmuir 16 (2000) 2398–2400.
[11] T.G. Schaaff, D.A. Blom, Nano Lett. 2 (2002) 507–511.
[12] H. Einaga, T. Ibusuki, S. Futamura, Environ. Sci. Technol. 38 (2004) 285–289.
[13] B. Sun, A.V. Vorontsov, P.G. Smirniotis, Langmuir 19 (2003) 3151–3156.
[14] S. Kim, W. Choi, J. Phys. Chem. B 106 (2002) 13311–13317.
[15] S. Jeon, P.V. Braun, Chem. Mater. 15 (2003) 1256–1263.
[16] X.P. Zhao, J.B. Yin, Chem. Mater. 14 (2002) 2258–2263.
[17] O. Diwald, T.L. Thompson, T. Zubkov, E.G. Goralski, S.D. Walck, J.T. Yates Jr., J. Phys. Chem. B 108 (2004) 6004–6008.
[18] M. Mrowetz, W. Balcerski, A.J. Colussi, M.R. Hoffmann, J. Phys. Chem. B 108 (2004) 17269–17273.
[19] S. Klosek, D. Raftery, J. Phys. Chem. B 105 (2001) 2815–2819.
[20] A. Patra, C.S. Friend, R. Kapoor, P.N. Prasad, Chem. Mater. 15 (2003) 3650–3655.
[21] J. Premkumar, Chem. Mater. 16 (2004) 3980–3981.
[22] J.D. Bryan, S.M. Heald, S.A. Chambers, D.R. Gamelin, J. Am. Chem. Soc. 126 (2004) 11640–11647.
[23] W. Choi, A. Termin, M.R. Hoffmann, J. Phys. Chem. 98 (1994) 13669–13679.
[24] M.I. Litter, J.A. Navío, J. Photochem. Photobiol. A 98 (1996) 171–181.
[25] J.A. Navío, G. Colón, M.I. Litter, G.N. Bianco, J. Mol. Catal. A 106 (1996) 267–276.
[26] K.T. Ranjit, B. Viswanathan, J. Photochem. Photobiol. A 108 (1997) 79–84.
[27] J.A. Navío, G. Colón, M. Macías, C. Real, M.I. Litter, Appl. Catal. A 177 (1999) 111–120.
[28] J.A. Navío, J.J. Testa, P. Djedjeian, J.R. Padrón, D. Rodríguez, M.I. Litter, Appl. Catal. A 178 (1999) 191–203.
[29] N. Uekawa, Y. Kurashima, K. Kakegawa, Y. Sasaki, J. Mater. Res. 15 (2000) 967–973.

[30] J. Araña, O. González-Díaz, M. Miranda-Saracho, J.M. Doña-Rodríguez, J.A. Herrera-Melián, J. Pérez-Peña, Appl. Catal. B 32 (2001) 49–61.
[31] J.Q. Wang, B.F. Xin, H.T. Yu, Z.Y. Ren, P.F. Qu, H.G. Fu, Chem. J. Chin. U. 24 (2003) 1093–1096.
[32] J.Q. Wang, B.F. Xin, H.T. Yu, Y.T. Xie, B. Zhao, H.G. Fu, Chem. J. Chin. U. 24 (2003) 1237–1240.
[33] H.G. Fu, J.Q. Wang, Z.Y. Ren, P.F. Yan, H.T. Yu, B.F. Xin, F.L. Yuan, Chem. J. Chin. U. 24 (2003) 1671–1676.
[34] J. Araña, J.M. Doña-Rodríguez, O. González-Díaz, E.T. Rendón, J. Mol. Catal. A 215 (2004) 153–160.
[35] J.F. Zhu, W. Zheng, B. He, J.L. Zhang, M. Anpo, J. Mol. Catal. A 216 (2004) 35–43.
[36] L. Kronik, Y. Sapira, Surf. Sci. Rep. 37 (1999) 1–206.
[37] Q.Z. Zhai, S.L. Qiu, F.S. Xiao, Z.T. Zhang, C.L. Shao, Y. Han, Mater. Res. Bull. 35 (2000) 59–73.
[38] X.M. Qian, X.T. Zhang, Y.B. Bai, T.J. Li, X.Y. Tang, E.K. Wang, S.J. Dong, J. Nanopart. Res. 2 (2000) 191–198.
[39] H.C. Gatos, J. Lagowski, R. Banisch, Photogr. Sci. Eng. 26 (1982) 42–49.
[40] L.Q. Jing, X.J. Sun, J. Shang, W.M. Cai, Z.L. Xu, Y.G. Du, H.G. Fu, Sol. Energ. Mat. Sol. C. 79 (2003) 133–151.
[41] G.P. Smestad, M. Gratzel, J. Chem. Educ. 75 (1998) 752–756.
[42] T. Ohsaka, S. Yamaoka, O. Shimomura, Solid State Commun. 30 (1979) 345–347.
[43] P.F. Yan, J.Q. Wang, X. Jiang, D.R. Zhou, H.G. Fu, Mater. Sci. Technol. 10 (2002) 28–31.
[44] X.M. Qian, H.H. Lű, X.T. Zhang, Y.S. Li, Y.B. Bai, T.J. Li, X.Y. Tang, Acta Sci. Nat. Univ. Jilin 2 (1999) 87–92.
[45] X.T. Zhang, Y.A. Cao, S.H. Kan, Y.M. Chen, J. Tang, H.Y. Jin, Y.B. Bai, L.Z. Xiao, T.J. Li, B.F. Li, Thin Solid Films 327–329 (1998) 568–570.
[46] J.M. Kesselman, G.A. Shreve, M.R. Hoffmann, N.S. Lewis, J. Phys. Chem. 98 (1994) 13385–13395.
[47] H. Liu, S.A. Cheng, M. Wu, H.J. Wu, J.Q. Zhang, W.Z. Li, C.A. Cao, J. Phys. Chem. A 104 (2000) 7016–7020.